

Breaking criterion and characteristics for solitary waves on slopes

S.T. Grilli¹, Member ASCE, I.A. Svendsen², Member ASCE, and R. Subramanya³

Abstract : Shoaling and breaking of solitary waves is computed on slopes 1:100 to 1:8 using an experimentally validated fully nonlinear wave model based on potential flow equations. Characteristics of waves are computed at and beyond the breaking point, and geometric self-similarities of breakers are discussed as a function of wave height and bottom slope. No wave breaks for slopes steeper than 12°. A breaking criterion is derived for milder slopes, based on values of a nondimensional slope parameter S_o . This criterion predicts both whether waves will break or not and which type of breaking will occur (spilling, plunging, or surging). Empirical expressions for the breaking index and for the depth and celerity at breaking are derived based on computations. All results agree well with laboratory experiments. The NSW equations fail to predict these results with sufficient accuracy at the breaking point. Pre-breaking shoaling rates follow a more complex path than previously realized. Post-breaking behaviors exhibit a rapid (non-dissipative) decay, also observed in experiments, associated with a transfer of potential energy into kinetic energy. Wave celerity decreases in this zone of rapid decay.

Keywords : Solitary wave propagation; wave shoaling; wave breaking; wave runup on beaches; long wave theory; fully nonlinear waves; experimental modeling of waves; numerical modeling of waves; boundary element method.

¹Associate Professor, *Department of Ocean Engineering*, University of Rhode Island, Narragansett, RI 02882. Tel.: (401) 874-6636

²Professor, *Center for Applied Coastal Research*, University of Delaware, Newark, DE 19716. Tel. : (302) 831-2441

³Graduate Research Assistant, same address as in 1.

Introduction

Recent advances in two-dimensional (2D) fully nonlinear wave models based on potential flow theory (e.g., Grilli *et al.*, 1989; Grilli, 1993) (FNPM) have made it possible to calculate “numerically exact” solutions for arbitrary waves shoaling over a complex bottom geometry ⁴.

Early FNPM were limited to deep water periodic waves (e.g., Longuet-Higgins and Cokelet, 1976; Vinje and Brevig, 1981; Dold and Peregrine, 1986) and were mostly used to simulate and study characteristics of deep water plunging breakers. Using such a model, Dommermuth *et al.* (1988) provided a detailed confirmation of the validity of potential flow theory to describe deep water plunging breakers produced in an experimental tank. The authors concluded that “the calculated free surface elevations are almost indistinguishable from measured profiles”.

Recent FNPM combining wave generation and absorption/radiation truly represent “numerical wave tanks” in which (numerical) experiments can be set-up and used to gain physical insight into complex wave phenomena like shoaling and breaking over a slope (e.g., Subramanya and Grilli, 1994; Grilli and Horrillo, 1996). Although periodic waves can be, and have been, used in such experiments, solitary waves have often been used instead, first of all due to their intrinsic interest as a good model of both tsunamis and very long nearshore waves ⁵, and also because they are much simpler to deal with in a FNPM than periodic waves ⁶. Motivations for such studies can be found mostly in the needs of coastal engineers for accurate predictions of height and location of breaking waves, and in the needs of surf-zone modelers for detailed characteristics of waves at the breaking point (BP), to be used as a forcing for surf-zone dynamics and sediment transport models (e.g., radiation stresses, crest height and celerity, particle kinematics; e.g., Svendsen *et al.*, 1978). Another important use of FNPM results is for the validation of approximate wave theories, like the recent study by Wei *et al.* (1995) in which standard and fully nonlinear Boussinesq models (FNBM) were compared to FNPM results used as a reference.

Thus, using a 2D FNPM, Grilli *et al.* (1994) calculated shoaling of solitary waves over a 1:35 slope and showed that surface elevations agreed to within 1% with high accuracy laboratory experiments, up to and slightly beyond the BP defined as the location where *the wave front face has a vertical tangent* (this is also usually the definition of the BP in laboratory experiments). Such an agreement indicates, as was already pointed out by Camfield and Street (1969), that, on a mild slope, bottom friction and other dissipative effects—not included in the FNPM—are not important for solitary wave shoaling. The same results also showed that exact shoaling rates significantly differ from predictions of both Green’s and Boussinesq’s laws and that horizontal velocities become very non-uniform over depth, as depth decreases, unlike predictions of nonlinear shallow water equations (NSW). This also causes the wave celerity at the BP to significantly differ from predictions

⁴Three-dimensional (3D) FNPM were also developed but such calculations are still considered computationally prohibitive (Broeze, 1993).

⁵Raichlen and Papanicolaou (1988), for instance, comment based on their experimental results that there are “striking similarities between these (cnoidal and solitary) two types of breaking waves”.

⁶Periodic waves require the implementation of an absorbing beach if one does not want to interrupt computations at the time of impact of a breaker jet on the free surface (e.g., Grilli and Horrillo, 1996).

of NSW equations (the last points will be further substantiated in the present study).

From the earlier work discussed above, it appears that potential flow theory can quite well predict the physics of wave shoaling over a slope, up to and into the early stages of breaking, before touch down of the breaker jet on the free surface. Hence, a FNPM can be used to investigate detailed characteristics of breaking waves, provided great care is taken in the numerical model to ensure high numerical accuracy of results. Because of the easy access to computed results, information can readily be obtained for flow details, such as those during the formation of the overturning jet of a wave, that are very difficult to accurately measure in laboratory experiments.

The present paper represents the second part of studies reported in Grilli *et al.* (1994), in which Grilli *et al.*'s (1989) FNPM was used to calculate characteristics of solitary waves shoaling over plane slopes. In the present paper, a much more accurate version of this model is used to compute detailed characteristics of solitary wave breakers, like jet shape and wave height variation, throughout early breaking (i.e., from the BP onward). Computations are carried out for a wide range of slopes and wave heights and results are used to derive both a breaking criterion and equations for predicting wave characteristics at breaking. Numerical results are validated by comparison with laboratory experiments ⁷.

More complete literature reviews and description of solitary waves shoaling and breaking characteristics may be found in the works by Camfield and Street (1969), Skjelbreia (1987), Synolakis (1987), Raichlen and Papanicolaou (1988), and Zelt (1991).

Description of the numerical model

Governing equations, boundary conditions, and numerical schemes for the present FNPM can be found in Grilli *et al.* (1989) and in Grilli (1993), and a summary of these is given in Appendix I. Fig. 1 shows a typical sketch of computational domain for solitary waves propagating over a slope s . Only the important aspect of accuracy of computations is briefly discussed hereafter.

Numerical accuracy.— In the present computations, to achieve sufficient accuracy both for highly nonlinear waves propagating over gentle slopes (i.e., over long distances) and for small scale breaker jets, three levels of improvements of the initial Grilli *et al.*'s model were needed : (i) a higher-order representation of both the free surface geometry and kinematics, ensuring continuity of the slope (“Mixed Cubic Interpolation method”; Grilli and Subramanya, 1996); (ii) selective and adaptive node regridding techniques allowing a higher resolution of computations in breaker jets and also preventing nodes from moving too close to each other (Grilli and Subramanya, 1996); and (iii) adaptive quasi-singular integration methods accounting for the proximity of nodes in breaker jets (Grilli and Subramanya, 1994).

Accuracy is checked in the present computations by verifying global conservation of wave

⁷The present study will only deal with waves that break during runup. It turns out that solitary waves that do not break during runup may still do so during run-down. This was pointed out by Synolakis (1987) and was also predicted in the computations by Svendsen and Grilli (1990) and Otta *et al.* (1993), using a FNPM.

volume and total energy (Grilli *et al.*, 1989). In all cases, spatial and temporal discretizations are selected for both errors on wave energy and volume to stay smaller than 0.05% during most of the wave propagation (see Grilli and Subramanya, 1996, for details of typical discretizations, numerical parameters, and computational errors for solitary wave shoaling). When breaker jets are forming, however, errors in volume and energy increase in the initial discretization. These errors are reduced by improving the resolution in breaker jets through addition and regridding of discretization nodes. Due to the smaller distance between nodes in regridded breaker jets, the (adaptive) time step very much reduces beyond the BP, which further improves computational accuracy. In the present applications, computations were stopped when global errors became larger than 1.0%. This criterion usually allowed following the development of breaker jets up to impending touch down on the free surface ⁸.

Shoaling and breaking of solitary waves over a slope

The first problem addressed in this paper is the question of how do solitary waves behave immediately before and after the breaking point (BP), as a function of both incident wave height and beach slope, with particular attention paid to breaker shape and self-similarity, and to pre- and post-breaking variation of the wave heights.

Breaker shape and self-similarity.— Figs. 2-5 show computations for the shoaling and breaking of solitary waves on plane beaches with slopes, $s = 1:100, 1:35, 1:15,$ and $1:8$. Three different incident wave heights, $H'_o = H_o/h_o$, are shown for each slope. Earlier studies by Grilli *et al.* (1994) concentrated on the shoaling aspects (illustrated in Fig. 1) and were carried out with a version of the model that was not able to pursue computations with sufficient accuracy further than the BP (represented by curves a in Figs. 2abc, 3abc, 4abc, 5c, and curve d in Fig. 5b). The new improvements of the model by Grilli and Subramanya (1994, 1996) allow computations to be pursued beyond the BP, almost up to touch-down of the breaker jets on the free surface without the model showing signs of break down (curves d in the same figures). Data and times, $t' = t\sqrt{g/h_o}$, of plotted curves a to d for the cases in Figs. 2-5 are given in Table 1. Unfortunately no experimental data are available for the details of the flow at this critical moment of the breaking.

Results in parts (a), (b), and (c) of Figs. 2-4 show that, for a given wave, a decrease in jet-size occurs as the slope decreases ⁹. On the (smallest) 1:100 slope, waves overturn with a fairly small size plunging jet (for $H_o \geq 0.40$, the jet touches down less than half the wave height down the slope; this is even more clear in Fig. 6 discussed below). On the other hand, Figs. 2-4 also show that the size of the jet does not change relative to the wave height for waves with different incident height on a given slope.

⁸Note that no local error check was used but various numerical methods used in the computations, particularly the node regridding technique combined to the adaptive time stepping scheme, were tested for convergence and stability by Grilli and Subramanya (1996).

⁹Jet size is defined here as the vertical distance between wave crest and jet tip.

This suggests that, for a fixed initial wave height, the height of the jet would tend to zero as the slope tends to zero. On a very gentle slope, the wave would propagate for long distances before reaching breaking, in a manner similar to the instability of the almost highest solitary wave on constant depth analyzed by Tanaka *et al.* (1987). Its breaker height would thus be very close to the maximum stable wave height on a horizontal bottom ($\simeq 0.78h_o$). Based on the present computations, our conjecture would be that, in this case, the breaking would still be plunging but at first on a very small scale. After touch-down of the (small) jet, however, the turbulent region would propagate down the slope in a situation that is usually associated with a spilling breaker.

The implication of this hypothesis is that all (so-called) spilling breakers actually start as (small scale) plunging breakers. High speed laboratory photographs by Papanicolaou and Raichlen (1987) (PR) and Raichlen and Papanicolaou (1988) (RP), of solitary waves breaking over a (very gentle) 1:164 slope, support this hypothesis and show that a very small scale curl-up of the wave crest occurs just before the bore usually associated with spilling breaking is observed. Local analytic solutions of potential flow equations by Jenkins (1994) also indicate the occurrence of very small size jets and that spilling and plunging breaking can be “regarded as being basically the same phenomenon except with a smaller length scale”¹⁰. Hence, for convenience, we have chosen here (arbitrarily) to use the term spilling breaker for a plunging breaker with a jet height less than half the wave height. Based on this criterion, the waves in Figs. 2bc represent spilling breakers while the waves in Figs. 2a, 3abc, and 4abc represent plunging breakers.

After reaching a vertical tangent at the BP (curves a in Figs. 2-4), breaking waves propagate for 1 to $3h_o$ in horizontal distance, depending on H'_o and s , before the jets impact the free surface (curves d in the figures). Propagation distances on this order can also be seen in PR and RP’s experiments.

On the steepest slope (1:8; Fig. 5), waves behave radically different from the plunging breakers in Figs. 2-4. As will be seen in Fig. 10, we are here at the limit between breaking and non-breaking waves. The wave in Fig. 5b ($H'_o = 0.40$) will eventually break as a surging breaker in which the vertical tangent of the front occurs at the toe. In Fig. 5a ($H'_o = 0.20$), the wave front never becomes quite vertical and the wave just runs up the slope without breaking. In Fig. 5c ($H'_o = 0.60$), computations were stopped at profile d but this case seems likely to develop into a collapsing breaker in which the toe shoots forward in spite of the already overhanging front.

Figs. 2-5 (a to c) indicate a fairly strong similarity between breakers for different waves on the same slope. To make it easier comparing breakers, parts (d) of Figs. 2-5 show a superposition of breaker shapes scaled in elevation by the incident wave height H_o and horizontally translated to the location x_c of breaker crests. Breakers correspond to curves d for the three different wave heights in each figure (note that in Fig. 5a curve a has been used to show the (non-breaking) wave shape just before it starts running up). We see that, on the same slope, breaking waves of different incident heights have a similar shape. The most important differences are that, the smaller the

¹⁰Note that recent experimental evidence by Duncan *et al.* (1994) suggests that when the scale of the instability that leads to breaking becomes sufficiently small, capillary effects dominate leading directly to a (small) turbulent roller without an overturning jet. Such small scales of instability, however, have not been investigated in this paper.

incident wave, the higher and more peaked the breaking wave and these differences become more pronounced the milder the slope. This implies that, on a given slope, the breaking index, H_b/h_b , is larger the smaller the incident wave. An equivalent similarity in shape is not found for waves of same incident height on different slopes. In Fig 6, we see that the overturning jets grow both in length and thickness as the slope becomes steeper (curves a to d). In all cases (except for curve d in Fig. 6a, the runup case), we are technically looking at plunging breakers (although some have formally been termed spilling as mentioned earlier) but it is obvious that a significant increase in the intensity of breaking takes place when the slope increases. On the basis of this observation, it would seem reasonable to consider the area of the jet at the instant of touch down as a measure of the strength of breaking. A dimensionless parameter could be obtained by dividing this area, say, by HL or H^2 .

Wave height variations before and after breaking.— Fig. 7 shows wave height variations as a function of depth $h(x')$, for the cases in Figs. 2-5. We see, again, that the slope is more significant than the incident wave height in determining changes in H up to and beyond the BP (symbols (o)).

Before the BP, wave height variations confirm the patterns discussed in Grilli *et al.* (1994) : (i) for all slopes, no wave has a real tendency to follow Green's law¹¹, $G \equiv H \propto h^{-1/4}$; (ii) for gentle slopes, Boussinesq law, $B \equiv H \propto h^{-1}$, only frames the results and, in average, no wave grows faster than $1/h$; (iii) on the steeper (1:8) slope, wave height essentially does not change and even slightly decreases towards the BP.

The more accurate model used in the present studies allows computations to be accurately pursued beyond the BP. One thus sees that, on the gentler slopes, wave height rapidly decreases over a short distance before touch-down of the jet. Since there is no dissipation in the FNPM, this decrease in height must entirely be due to a reorganization of potential energy into kinetic energy in the wave. This is easily confirmed by computing these quantities in the FNPM (which cannot readily be determined from experiments). Computations show that, even before the BP, potential energy starts slowly transforming into kinetic energy (see, e.g., Fig. 7 in Grilli *et al.*, 1994). Due to the increasing wave asymmetry during shoaling (Fig. 1), however, despite the decrease in potential energy, the crest elevation still increases up to the BP while the back of the wave spreads out and flattens. Beyond the BP, results show that the transformation of potential into kinetic energy accelerates due to the large particle velocities associated with the plunging jet (see, e.g., Fig. 6 in Grilli *et al.*, 1994). This leads to the rapid decrease observed in wave height.

Synolakis and Skjelbreia (1993) (SS), based on experimental results for mild slopes ($s \leq 1:50$), identified a *zone of rapid decay* for the wave height beyond the BP where, $H \propto h^\alpha$. Present FNPM results give an average $\alpha = 2.7, 1.7, \text{ and } 0.84$, for the 1:100, 1:35, and 1:15 slopes, respectively, i.e., smaller than the value $\alpha = 4$ found by SS. The latter value, however, averaged both dissipative and non-dissipative effects and a smaller rate of decay in FNPM computations should thus be expected. PR and RP provided detailed measurements of wave height variations beyond the BP for solitary waves breaking on mild slopes. In PR-RP's results, it is clear that wave height initially

¹¹Except maybe for part of the shoaling on a slope that would be about 1:15, but this would be considered fortuitous.

decreases over a horizontal distance about $2-8 h_b$ beyond the BP (almost linearly in a log-log diagram). At this point, wave height starts more strongly decreasing. Comparing these wave height variations to the photographs also given in PR-RP's study, it can be conjectured that the initial wave height decrease observed in experiments represents the non-dissipative wave height reduction calculated in the FNPM, corresponding to jet development before touch down, whereas the stronger subsequent reduction is due to dissipations throughout breaking. Based on the curves in PR-RP's study, one can estimate $\alpha \simeq 1.95$ for the initial wave height decrease beyond the BP on a 1:52 slope, which is within the range obtained in the present computations.

Breaking criterion and prediction of breaking characteristics

The second problem addressed in this paper is the question of which waves break on which slopes and with which characteristics, with particular attention paid to the transition to breaking, the breaking criterion, and to the breaking indices, depths, and types.

Transition to breaking.— Computations in Figs. 2-5 showed that, on a given slope, breaking may or may not occur and breaker types may differ depending on both incident wave height H'_o and slope s . Results of these computations are summarized in Fig. 10 along with many other similar numerical results obtained both here and in previous studies by Grilli *et al.* (1994) and Otta *et al.* (1993) (see Table 1). The figure shows which waves break and which do not. Breaker types (spilling (SP), plunging (PL), or surging (SU)), also marked on the figure, are discussed in the next Section. We see first of all that a very large wave with $H'_o = 0.75$ (i.e., close to the maximum stable height $\simeq 0.78$; Tanaka, 1986), does not break if the slope is too steep ($s = 1:1.73, 1:4$), whereas the wave does break on the milder slopes ($s = 1:8$ and $1:15$)¹². For smaller waves, the figure clearly shows a limit between breaking and non-breaking solitary waves that depends on the slope and, in the log-log plot for $(H'_o, 1/s)$, shows up as a linear dependence between $\log H'_o$ and $\log 1/s$ (bold solid line in Fig. 10). To more exactly locate this limit and to better understand the transition between breaking and non-breaking waves, numerical experiments were carried out on a few different slopes, for waves with height that was incrementally increased across this line.

Figs. 8 and 9 present some of these calculations for 1:15 and 1:8 slopes, respectively, and for three different wave heights for each slope : (i) in part (a), a non-breaking wave height (i.e., below the limit in Fig. 10); (ii) in part (b), a wave height that is barely breaking (i.e., on the limit in Fig 10); (iii) in part (c), a clearly breaking wave (i.e., above the limit). Parts (d) of the figures show a comparison between the first (non-breaking) profiles (curves a) in part (a) and the last (breaking) profiles (curves d) in parts (b) and (c) of the figures, each scaled by the incident wave height. Data and times t' for curves a to d for cases in Figs. 8 and 9 are given in Table 1. (Several similar

¹²The question of whether such a large wave would occur or not in nature or, more precisely, would be stable for long enough to reach a beach slope, has not been addressed here. These waves are predicted to exist within the frame of FNPM's, both numerical and semi-analytical (e.g., streamfunction theory), and are thus relevant to the present study. Besides, results for large waves certainly do not undermine or contradict our conclusions for smaller waves.

computations with small wave height increments—not reported here—were performed for other slopes as well, to determine the exact position of the line in Fig 10).

Both cases in Figs. 8b and 9b appear to break as surging/collapsing breakers for which no crest overturning actually occurs but the whole wave collapses on itself before surging up the slope. To determine which waves were actually breaking and which were not, we checked if we could calculate a complete runup/run-down cycle without disturbance or break down of the water surface.

The barely breaking profiles in Figs. 8b and 9b show a marked increase in the slope of the wave front face, as compared to the non-breaking profiles in Figs. 8a and 9a (see also parts (d)). The slope never becomes completely vertical, however, and it is conjectured that there is a non-vertical value of this slope which defines the point of transition to breaking. A closer investigation of this, however, requires more computations for a more detailed analysis of the wave kinematics close to the point of intersection of the water surface with the slope, and will have to be left out for further studies.

Cases in Figs. 8b and 9b can be identified in Fig. 10, as delimiting part of the breaking limit. Characteristics of the latter are further discussed in the following section.

Breaking criterion, breaking type.— The limit between breaking and non-breaking solitary waves, i.e., the *breaking criterion* (represented by the bold solid line in Fig. 10), was determined using a Least Square method based on the calculations, as,

$$H'_o > 16.9 s^2 \tag{1}$$

which indicates that incident solitary waves satisfying (1) will break sometime during runup on a slope s .

Many past studies have attempted to define breaking criteria and breaking characteristics for solitary waves on plane slopes. Camfield and Street (1969) (CS) concluded, on the basis of their experiments and of experiments by Ippen and Kulin (1954), that “there was no evidence of breaking” for slope angles larger than 12° (or, $s > 1:4.7$). This fully agrees with the criterion (1) which predicts that a wave of maximum height, $H'_o = 0.78$, will only break for $s < 1 : 4.7$.

A different criterion was found by Synolakis (1987). Using the NSW equations, he suggested that waves would eventually break during runup if, $H'_o > 0.818 s^{10/9}$. This criterion is indicated by the dashed line in Fig. 10, and we see that the NSW equations predict that much smaller waves will break than found using the present more accurate method ¹³ (this could be expected as a result of the shallow water steepening occurring in the non-dispersive NSW equations). NSW equations

¹³For waves of sufficiently small height (such as tsunamis), the extrapolation of the two criteria in Fig. 10 will intersect for, $H'_o = 0.019$ and $s = 1:30$. Hence, only for one wave height on one slope would the NSW and FNPM methods give the same limit but it is not clear, however, that equation (1) could be extrapolated to such small values of H'_o , for which we have not at the present time performed any numerical experiments. Besides, even such small waves will become quite steep when they approach breaking, which means the NSW approximation breaks down. Near breaking, the deviation from the hydrostatic pressure assumed in the NSW equations is important for the wave development.

were shown in a number of studies to quite well predict the runup value for non-breaking solitary waves on mild slopes (e.g., Synolakis, 1987). Since runup is greatly reduced if waves break, however, the prediction of breaking for waves that actually do not break also means that the NSW equations predict much less runup for this class of non-breaking waves.

Non-dimensional parameters are usually used to predict breaking waves characteristics. A surf-similarity-type parameter would be a possible candidate (Yasuda *et al.*, 1992). Here, we will use the slope parameter S_o , defined as sL_o/h_o where L_o is a characteristic horizontal length scale for the initial wave. The question remains which wave length scale L_o to use for a solitary wave. Raichlen and Papanicolaou (1988) suggested to use the width of the incident solitary wave at a height $H_o/2$ above still water level. In the present study, following Klitting and Svendsen (1974), this width is measured between the points of maximum slope on the solitary wave profile. Using Boussinesq's solitary wave theory, we thus get,

$$L_o = \frac{2h_o}{\sqrt{3H_o'/4}} \operatorname{arctanh} \frac{\sqrt{3}}{3} \quad (2)$$

and the slope parameter S_o for solitary waves is then defined as,

$$S_o = \frac{sL_o}{h_o} = 1.521 \frac{s}{\sqrt{H_o'}} \quad (3)$$

Incidentally this parameter has a 99.9% correlation with the parameter, $\xi_s = s/H_o'^{0.4}$, introduced by Yasuda *et al.* (1992) on a heuristic basis.

Combining (1) and (3), we see that criterion (1) for occurrence of breaking simply corresponds to $S_o < 0.37$. In Fig. 10, a family of lines corresponding to $S_o = 0.025$ to 0.80, has been plotted and we see that (1) is almost identically represented by, $S_o < 0.37$. Values of S_o for the calculations in Figs. 2-5 and 8,9 are given in Table 1. One can see, in particular, that the barely breaking waves shown in Figs. 8b and 9b have, as expected, $S_o \simeq 0.37$. Now, referring to the breaking types marked by various symbols in Fig. 10 and listed in Table 1, one can also see that they can be predicted in terms of values of the parameter S_o as,

- i) surging breaking : $0.3 < S_o < 0.37$
- ii) plunging breaking : $0.025 < S_o < 0.30$
- iii) spilling breaking : $S_o < 0.025$

Hence, using one single parameter S_o , we can predict whether a solitary wave will break or not on a given slope and which type of breaking will occur. Wave characteristics at breaking are discussed in the next sections.

Breaking index and breaking depth.— The simple limit, $H_b/h_b \simeq 0.80$, corresponding to the maximum stable solitary wave in constant depth, has been and is still often used as a breaking

index for both solitary and long periodic waves breaking over very mild slopes. To improve on this value, CS proposed an empirical breaking index for solitary waves, based on an average of their experimental results and of those by Ippen and Kulin (1954), for all wave heights on a given slope,

$$H_b/h_b = 0.75 + 25s - 112s^2 + 3870s^3 \quad (4)$$

Results of our computations can be used to derive a similar, albeit improved, relationship. Using a Least Square method for the results of computations in Figs. 2-5, and 8,9, summarized in Table 1, along with results of other computations by Grilli *et al.* (1994) and Otta *et al.* (1993), also summarized in Table 1, we get.

$$H_b/h_b = 0.841 \exp(6.421 S_o) \quad (5)$$

with a correlation coefficient ¹⁴, $R = 0.997$. Similarly, for the breaking depth, we get h_b/h_o as a function of S_o/H'_o , for SP and PL breakers, as,

$$h_b/h_o = \frac{0.149}{(S_o/H'_o)^{0.523}} \quad \text{with} \quad S_o < 0.30 \quad (6)$$

and for SU breakers, as,

$$h_b/h_o = \frac{0.0508}{(S_o/H'_o)^{1.00}} \quad \text{with} \quad 0.30 < S_o < 0.37; S_o/H'_o > 0.385 \quad (7)$$

with correlation coefficients, $R = 0.967$ and 0.995 , respectively.

An extensive collection of experimental data is available for the breaker index and breaker depth of solitary waves (PR, for 1:52 to 1:164 slopes; Skjelbreia (1987), for 1:52 to 1:161 slopes; CS, for 1:33 to 1:100 slopes; and Grilli *et al.* (1994), who reported experiments by Veeramony and Svendsen (1994) for a 1:35 slope). These results are all listed in Table 2 and compared ¹⁵ in Fig. 11 to values predicted by eqs. (5), (6) and (7), along with numerical data from Table 1. Notice that there are no experimental data for SU breakers ¹⁶. We see that the empirical expressions represent both the numerical and the experimental data very well. It is also seen that types of breaking in each experiment agree with the numerical predictions. More importantly, however, we observe that, when plotted as a function of S_o , the data for all slopes and wave heights collapse into one single curve for the breaking index in Fig. 11a. This even applies to the numerical data for SU and one sees that the maximum breaking index, beyond which waves are non-breaking (NB), is 9.05 for a SU breaker, with $S_o = 0.37$. Similarly, the parameter S_o/H'_o makes all data for h_b/h_o fall on

¹⁴A similar result was obtained for periodic waves by Svendsen (1987). Because of the use of the conventional wave length for L_o in that work and the use of parameters at the break point, the two results are not directly comparable.

¹⁵To facilitate the comparison, the experimental data have been fitted to expressions similar to (5) and (6), and the results are shown as dashed curves in Fig. 11.

¹⁶For the breaker index in Fig. 11a, the data available from numerical and physical experiments does not make it possible to distinguish different laws for the two radically different breaking processes of PL and SU. For this, more data would be needed in the interval of S_o between 0.2 and 0.3. In Fig. 11b, on the other hand, the two processes clearly distinguish themselves in the h_b/h_o data.

the same curves in Fig. 11b. No other representation is capable of this. Note, however, that h_b is measured as the undisturbed depth under the wave crest (see Fig. 1) and as this depth becomes very small when we approach large values of S_o , results obviously become similarly uncertain.

The breaking index relationship (5) is compared in Fig. 12a to CS's experimental criterion (4). It is immediately seen that, because CS's (dashed) expression uses s rather than S_o , it cannot account for the influence of wave height on a given slope¹⁷, which is rather significant for average to steep slopes (curves a-h). It is noticed, however that for very gentle slopes (1:100 or less; S_o very small) both criteria (5) and (4) predict breaker indices close to the constant depth limit of $H_b/h_b \simeq 0.80$, with no noticeable influence of slope or wave height. Now, considering that CS's average criterion falls in the middle of the values predicted by criterion (5) for wave heights ranging between $H'_o = 0.05$ and 0.78, the agreement between both criteria is, hence, fairly reasonable. Fig. 12b, finally, summarizes the present findings for both breaking indices and breaking types as a function of $(H'_o, 1/s)$, in a form that allows for easy prediction for given incident solitary wave height and slope.

Wave celerity at breaking.— The crest celerity c'_b at breaking is given in Table 1 for the computations in Figs. 2-5, along with the ratio c'_{bs}/c'_b in which the numerator denotes the celerity predicted by NSW equations¹⁸, $c'_{bs} = \sqrt{H'_b + h'_b}$, which is often used in surf-zone models to estimate wave celerity at breaking. Computations show that : (i) on the two milder slopes, wave celerity decreases during shoaling up to a point close to the BP and then increases up to the BP; (ii) on the two steeper slopes, celerity increases during shoaling up to the BP. In all cases, celerity rapidly decreases beyond the BP.

At the BP, results in Table 1 for c'_b show that, on the two milder slopes, the NSW equations mostly overpredict crest celerity (by up to 59%), the overprediction being larger for the smaller waves on the milder slope. The comparison of results of FNBM and FNPM results by Wei *et al.* (1995), for a range of slopes 1:100 to 1:8, showed that wave celerity is quite well predicted in the FNBM, except right at the BP where the FNBM slightly underpredicts celerity. Since the FNBM has fully nonlinear terms, as do NSW eqs., the larger discrepancies observed here with the NSW equations are thus likely due to a lack of dispersive effects in these equations (such observations were already made by Grilli *et al.*, 1994, on the basis of two computations). This is well supported by the larger discrepancies observed in Table 1 for the smaller waves shoaling over the milder slopes, for which the longer distances of propagation are likely to make dispersive effects increase. On the two steeper slopes, overprediction of celerity is less, with a maximum of 10%, but celerity is underpredicted in most cases (by up to 43%). These results, again, show the inadequacy of the NSW equations to describe wave kinematics close to the BP, where vertical accelerations (i.e., dispersive effects) and, hence, non-hydrostatic pressure increase.

¹⁷In fact, (4) was obtained by averaging experimental results for all wave heights on a given slope and thus lost wave height information.

¹⁸Note that the breaker height obtained in the FNPM was used in the NSW celerity equation. This is acceptable since NSW equations are known to predict wave elevations better than kinematics, but still represents an approximation.

An empirical expression was derived for c'_b based on results in Table 1. It was found that the only significant factor explaining the variation of c'_b was H'_o , with very little effect of slope. The expression thus reads,

$$c'_b = 0.466 + 2.58H'_o - 1.82H'^2_o \quad (8)$$

with a correlation coefficient, $R = 0.991$.

Conclusions

Summarizing the results, we conclude that :

- No wave that can propagate stably on a constant depth breaks on slopes steeper than 12° ($> 1 : 4.7$). With $S_o = sL_o/h_o$, waves break on a given slope : (i) as surging breakers (SU) when $0.30 < S_o < 0.37$ (with $5.8 < H_b/h_b < 9.1$); (ii) as plunging breakers (PL) when $0.025 < S_o < 0.30$ (with $1.0 < H_b/h_b < 5.8$); and (iii) as spilling breakers (SP) when $S_o < 0.025$ (with $H_b/h_b < 1.0$). For $s < 1:4.7$, waves do not break when $S_o > 0.37$. These results are supported by both computations and experiments. The NSW equations fail to predict which waves break and which do not.
- The most important parameter deciding the shape of breaking waves is the slope, the initial wave height being of secondary importance. Thus, breaker shapes are fairly self-similar on a given slope. On the milder slopes, however, breakers are more peaky and deformed for the smaller incident waves. Sizes of plunging jets for SP and PL increase significantly with the slope. SP and PL waves propagate for 1 to $3h_o$ beyond the BP, before their breaker jet hits the free surface.
- Shoaling rates for mild slopes ($s < 1:20$) increase monotonously towards breaking and may even increase faster than h^{-1} , the rate predicted by Boussinesq theory for solitary waves. Shoaling rates decrease dramatically with increasing slope steepness and, on steeper slopes ($> 1 : 15$), the rates are much lower than predicted by Green's law and can even be negative (i.e., wave height decreases towards the BP). Beyond the BP, wave height initially decreases with $H \propto h^{(2-3)}$. This (non-dissipative) decrease, also observed in experiments, is associated with a transformation of potential energy into kinetic energy in the wave, at an increased rate beyond the BP due to larger velocities in plunging jets. After touch-down of the jet, the FNPM is not applicable and experiments show that wave height decreases at a higher rate due to dissipations in the flow.
- For all slopes investigated here, the breaking index H_b/h_b is well above the limit of approximately 0.80 of the steepest stable wave on constant depth. This is also supported by experiments. For moderately steep slopes or very small waves (i.e., large $S_o < 0.37$), waves may break very close to the shoreline and the breaking index becomes very large (with a maximum of about 9 for h_b measured under the wave crest). On a given slope, the breaking index increases with the decreasing wave height.

- Empirical expressions (5)-(7) for the breaking index and the breaking depth, developed by curve fitting of the numerical results, agree well with experimental results and can be used to predict wave characteristics at breaking. Results for breaking criterion, breaker-type, and indices are summarized in Fig. 12b.
- Wave crest celerity decreases when waves propagate beyond the BP. At breaking, wave celerity is significantly over- or under-predicted by the NSW equations (by up to 59%), for mild or steep slopes, respectively. The empirical expression (8) can be used to predict wave celerity at breaking.

Acknowledgments

SG and RS wish to acknowledge support for this research from the NRL-SSC, grant N00014-94-1-G607, from the Department of the Navy, Office of the Chief of Naval Research. The information reported in this work does not necessarily reflect the position of the Government.

Appendix I—A review of FNPM governing equations

Equations and numerical methods for the FNPM are briefly reviewed here. Details can be found in Grilli *et al* (1989), Grilli (1993), and Grilli and Subramanya (1994, 1996). The velocity potential $\phi(\mathbf{x}, t)$ is used to represent inviscid irrotational 2D flows in the vertical plane (x, z) and the velocity is defined by $\mathbf{u} = \nabla\phi = (u, w)$ (Fig. 1). Continuity equation in the fluid domain $\Omega(t)$ with boundary $\Gamma(t)$ is a Laplace's equation for the potential

$$\nabla^2\phi = 0 \quad \text{in } \Omega(t) \quad (9)$$

Using free space Green's function, $G(\mathbf{x}, \mathbf{x}_l) = -(1/2\pi) \log |\mathbf{x} - \mathbf{x}_l|$, and Green's second identity, equation (9) transforms into the boundary integral equation (BIE),

$$\alpha(\mathbf{x}_l)\phi(\mathbf{x}_l) = \int_{\Gamma(\mathbf{x})} \left[\frac{\partial\phi}{\partial n}(\mathbf{x})G(\mathbf{x}, \mathbf{x}_l) - \phi(\mathbf{x})\frac{\partial G(\mathbf{x}, \mathbf{x}_l)}{\partial n} \right] d\Gamma(\mathbf{x}) \quad (10)$$

in which $\mathbf{x} = (x, z)$ and $\mathbf{x}_l = (x_l, z_l)$ are position vectors for points on the boundary, \mathbf{n} is the unit outward normal vector, and $\alpha(\mathbf{x}_l)$ is a geometric coefficient.

Equation (10) is solved by a boundary element method (BEM; Brebbia and Walker, 1978), using a set of collocation nodes on the boundary and higher-order elements to interpolate in between the collocation nodes. Integrals in (10) are numerically evaluated and the resulting algebraic system of equations is assembled and solved for the equivalent discretized problem.

Along the stationary bottom Γ_b , a no-flow condition is prescribed by

$$\frac{\partial\phi}{\partial n} = 0 \quad \text{on } \Gamma_b \quad (11)$$

Solitary waves are generated in the model, over a region of constant depth h_o , by simulating a piston wavemaker motion on the "open sea" boundary of the computational domain, $\Gamma_{r1}(t)$ (as in

laboratory experiments), or by specifying the potential ϕ normal velocity $\partial\phi/\partial n$ and the elevation η at initial time t_0 , for the incident wave, directly on the free surface (as in Tanaka, 1986).

On the free surface $\Gamma_f(t)$, ϕ satisfies the kinematic and dynamic boundary conditions,

$$\frac{D\mathbf{r}}{Dt} = \left(\frac{\partial}{\partial t} + \mathbf{u} \cdot \nabla \right) \mathbf{r} = \mathbf{u} = \nabla \phi \quad \text{on } \Gamma_f(t) \quad (12)$$

$$\frac{D\phi}{Dt} = -gz + \frac{1}{2} \nabla \phi \cdot \nabla \phi - \frac{p_a}{\rho} \quad \text{on } \Gamma_f(t) \quad (13)$$

respectively, with \mathbf{r} , the position vector on the free surface, g the gravitational acceleration, z the vertical coordinate, p_a the pressure at the free surface, assumed zero in the applications, and ρ the fluid density.

At a given time, computations in the model proceed forward in time by integrating the fully nonlinear free surface boundary conditions (12) and (13), using third-order accurate explicit Taylor series expansions for ϕ and \mathbf{r} , expressed in terms of a time step Δt and of the Lagrangian time derivative D/Dt . Terms in both series expansions are calculated by solving two BIE's of the type (10) for ϕ and $\partial\phi/\partial t$, in sequence at each time step, the solution of the first BIE providing boundary conditions for the second BIE. Trajectories of individual free surface particles — identical to nodes of the BEM discretization — are thus calculated as a function of time.

The time step in the model is adaptively selected based on a constant mesh Courant number (optimal value $\simeq 0.35 - 0.5$) to ensure optimal accuracy and stability of computations. Time step is thus reduced when the distance between free surface nodes decreases.

Appendix II—References

- Brebbia, C.A. and S. Walker (1978) *Boundary Element Techniques in Engineering*. Newnes-Butterworths, London.
- Broeze, J. (1993) *Numerical Modelling of Nonlinear Free Surface Waves With a 3D Panel Method*. Ph.D. Dissertation, Enschede, The Netherland.
- Camfield, F.E. and Street, R.L. (1969) "Shoaling of Solitary Waves on Small Slopes." *J. of Waterway Port Coastal and Ocean Engineering*, **95** (1), 1-22.
- Dold, J.W. and Peregrine, D.H. (1986) "An Efficient Boundary Integral Method for Steep Unsteady water Waves." In *Numerical methods for Fluid Dynamics II* (ed. K.W. Morton & M.J. Baines), pp. 671-679, Clarendon Press, Oxford.
- Dommermuth, D.G., Yue, D.K.P., Lin, W.M., Rapp, R.J., Chan, E.S. and Melville, W.K. (1988) "Deep-Water Plunging Breakers : a Comparison between Potential Theory and Experiments." *J. Fluid Mech.* **189**, 423-442.
- Duncan, J.H., Philomin, V., Behres, M. and J. Kimmel (1994) "The Formation of Spilling Water Waves." *Phys. Fluids* **6** (9).

- Grilli, S. (1993) "Modeling of Nonlinear Wave Motion in Shallow Water." Chapter 3 in *Computational Methods for Free and Moving Boundary Problems in Heat and Fluid Flow* (eds. L.C. Wrobel and C.A. Brebbia), pps. 37-65, Comp. Mech. Pub., Elsevier, London, UK.
- Grilli, S. and J. Horrillo (1996) "Numerical Generation and Absorption of Fully Nonlinear Periodic Waves." *J. Engng. Mech.* (accepted).
- Grilli, S., Skourup, J. and Svendsen, I.A. (1989) "An Efficient Boundary Element Method for Nonlinear Water Waves." *Engng. Analysis with Boundary Elements*, **6** (2), 97-107.
- Grilli, S.T. and Subramanya, R. (1994) "Quasi-singular Integrals in the Modeling of Nonlinear Water Waves in Shallow Water." *Engng. Analysis with Boundary Elements*, **13**, 181-191.
- Grilli, S.T. and Subramanya, R. (1996) "Numerical Modeling of Wave Breaking Induced by Fixed or Moving Boundaries." *Computational Mech.*, **17** (6), 374-391.
- Grilli, S.T., Subramanya, R., Svendsen, I.A., and Veeramony, J. (1994) "Shoaling of Solitary Waves on Plane Beaches." *J. Waterways Port Coastal Ocean Engng.*, **120** (6), 609-628.
- Ippen, A.T. and Kulin, G. (1954) "The Shoaling and Breaking of the Solitary Waves." In *Proc. 5th Intl. Conf. on Coastal Engineering* (ICCE5), pps. 27-47, ASCE edition, New York.
- Jenkins, A.D. (1994) "A Stationary Potential-flow Approximation for a Breaking Wave Crest." *J. Fluid Mech.* **280**, 335-347.
- Klinting, P. and I. A. Svendsen (1974) "A discussion of the characteristic horizontal lengths in long waves" *Inst. Hydrodyn. and Hydr. Eng., Tech. Univ of Denmark*, Prog. Rep. **34**, 11-17.
- Longuet-Higgins, M.S. and Cokelet, E.D. (1976) "The Deformation of Steep Surface Waves on Water - I. A Numerical Method of Computation." *Proc. R. Soc. Lond.* **A350**, 1-26.
- Otta, A.K., Svendsen, I.A., and Grilli, S.T. (1993) "The Breaking and Runup of Solitary Waves on Beaches." In *Proc. 23rd Intl. Conf. on Coastal Engineering* (ICCE23, Venice, Italy, October 92) Vol. **2**, pps. 1461-1474. ASCE edition, New York.
- Papanicolaou, P. and Raichlen, F. (1987) "Wave Characteristics in the Surf Zone." In *Proc. Coastal Hydrodynamics* (Univ. of Delaware, Newark, June 87) (ed. R.A. Dalrymple), pps. 765-780. ASCE edition, New York.
- Raichlen, F. and P. Papanicolaou (1988) "Some Characteristics of breaking Waves." In *Proc. 21st Intl. Conf. on Coastal Engineering* (ICCE21, Malaga, Spain, July 88) pps. 377-392. ASCE edition, New York.
- Skjelbreia, J.E. (1987) "Observations of Breaking Waves on Sloping Bottoms by Use of Laser Doppler Velocimetry." *W.M. Keck Laboratory of Hydraulics and Water Resources, California Institute of Technology, Report No.* **KH-R-48**.

- Subramanya, R. and Grilli, S.T. (1994) "Kinematics and Properties of Fully Nonlinear Waves Shoaling Over a Gentle Slope." In *Proc. Intl. Symposium on Waves - Physical and Num. Modelling* (Vancouver BC, Canada, Aug. 1994) (eds. M. Isaacson & M. Quick), Vol. **2**, pps. 1106-1115, IAHR.
- Svendsen, I.A. (1987) "Analysis of Surfzone Turbulence." *J. Geophysical Res.* **92**, 5115-5124.
- Svendsen, I.A., and Grilli, S.T. (1990) "Nonlinear Waves on Steep Slopes." *J. Coastal Research*, **SI 7**, 185-202.
- Svendsen, I.A., Madsen, P.A., and Hansen, J.B. (1978) "Wave Characteristics in the Surf Zone." *Proc. 16th Intl. Conf. on Coastal Engineering* (ICCE16, Hamburg, Germany) pps. 520-539, ASCE edition, New York.
- Synolakis, C.E. (1987) "The Runup of Solitary Waves." *J. Fluid Mechanics*, **185**, 523-545.
- Synolakis, C.E. and Skjelbreia, J.E. (1993) "Evolution of Maximum Amplitude of Solitary Waves on Plane Beaches." *J. Waterway Port Coastal and Ocean Engineering*, **119** (3), 323-342.
- Tanaka, M. (1986) "The Stability of Solitary Waves." *Phys. Fluids*, **29** (3), 650-655.
- Tanaka, M., Dold, J.W., Lewy, M. and Peregrine, D.H. (1987) "Instability and Breaking of a Solitary Wave." *J. Fluid Mech.* **185**, 235-248.
- Veeramony, J. and I. A. Svendsen (1994) In preparation.
- Vinje, T. and Brevig, P. (1981) "Numerical Simulation of Breaking Waves." *Adv. Water Res.* **4**, 77-82.
- Yasuda, T., Sakakibara, Y., and Hara, M. (1992) "BIM Simulation on Deformation up to Breaking of Solitary Waves over Uneven Bottoms." In *Proc. 4th Intl. Conf. on Hydraulic Engng. Software* (Valencia, Spain, July 92) (eds. W.R. Blain and E. Cabrera), Fluid Flow Modelling, pp. 523-535. Elsevier, Southampton.
- Wei, J., Kirby, J.T, Grilli, S.T. and R., Subramanya (1995) "A Fully Nonlinear Boussinesq Model for Surface Waves. I. Highly Nonlinear Unsteady Waves." *J. Fluid Mech.* **294**, 71-92.
- Zelt, J.A. (1991) "The Runup of Non-breaking and Breaking Solitary Waves." *Coastal Engineering*, **15**, 205-246.

Appendix III–Notations

c_b = breaking wave celerity (FNPM);
 c_{bs} = breaking wave celerity (NSW);
 g = gravitational acceleration;
 h = local water depth;
 h_b = water depth at breaking measured under the wave crest;
 h_o = constant reference water depth;
 s = beach slope;
 t = time;
 x = horizontal coordinate;
 x_b = location of the breaking point;
 z = vertical coordinate;
BP = breaking point;
FNBM = fully nonlinear Boussinesq model;
FNPM = fully nonlinear potential flow model;
 H = local solitary wave height;
 H_b = solitary wave height at breaking;
 H_b/h_b = breaking index;
 H_o = incident solitary wave height;
NB = non-breaking wave;
NSW = nonlinear shallow water;
PL = plunging breaking wave;
SP = spilling breaking wave;
SU = surging breaking wave;
 S_o = slope parameter;
 η = local wave amplitude;

Subscript

b = quantities at the breaking point;
 o = quantities for the incident wave;

Superscript

' (prime) = dimensionless variables according to long wave theory : lengths are divided by h_o , times by $\sqrt{h_o/g}$, and velocities and celerities by $\sqrt{gh_o}$.

Appendix IV—Tables

s	H'_o	S_o	H'_b	H_b/h_b	x'_b	c'_b	c'_{bs}/c'_b	t'_a	t'_b	t'_c	t'_d	Type
1:100	0.20	0.0340	0.361	1.066	66.13	0.878	1.586	66.93	68.16	69.13	69.89	PL
1:100	0.40	0.0240	0.629	1.041	39.56	1.213	1.154	34.37	35.47	36.20	36.77	SP
1:100	0.60	0.0196	0.781	1.033	24.46	1.351	1.038	19.41	20.26	21.20	21.73	SP
1:35	0.10	0.1370	0.203	1.950	31.36	—	—	—	—	—	—	PL
1:35	0.15	0.1120	0.296	1.473	27.96	—	—	—	—	—	—	PL
1:35	0.20	0.0972	0.364	1.402	25.90	0.943	1.388	25.91	26.74	27.40	27.80	PL
1:35	0.25	0.0870	0.422	1.385	24.29	—	—	—	—	—	—	PL
1:35	0.30	0.0790	0.476	1.380	22.93	—	—	—	—	—	—	PL
1:35	0.40	0.0687	0.592	1.378	19.97	1.231	1.067	17.10	17.80	18.44	19.04	PL
1:35	0.60	0.0561	0.754	1.312	14.89	1.364	0.973	11.60	12.29	12.72	13.10	PL
1:20	0.20	0.1701	0.332	2.104	16.84	—	—	—	—	—	—	PL
1:15	0.06	0.4140	—	—	—	—	—	17.11	17.54	18.31	19.14	NB
1:15	0.08	0.3650	0.099	8.735	14.83	—	—	15.51	15.89	16.22	16.48	SU
1:15	0.10	0.3210	0.111	6.660	14.75	—	—	15.38	15.76	16.01	16.20	SU
1:15	0.30	0.1851	0.398	2.651	12.75	1.064	1.103	11.43	11.86	12.19	12.52	PL
1:15	0.45	0.1512	0.556	2.372	11.48	1.229	0.970	9.29	9.87	10.35	10.73	PL
1:15	0.60	0.1309	0.689	2.180	10.26	1.342	0.900	7.78	8.61	9.18	9.41	PL
1:15	0.70	0.1210	0.820	1.970	8.72	—	—	—	—	—	—	PL
1:8	0.20	0.4251	—	—	—	—	—	7.54	8.03	8.53	9.03	NB
1:8	0.22	0.4050	—	—	—	—	—	6.58	8.16	9.19	10.21	NB
1:8	0.26	0.3720	0.291	9.100	7.74	—	—	5.19	5.98	6.39	6.54	SU
1:8	0.30	0.3470	0.321	8.050	7.68	—	—	5.41	5.73	6.00	6.34	SU
1:8	0.32	0.3360	0.346	7.395	7.63	—	—	—	—	—	—	SU
1:8	0.34	0.3260	0.362	7.005	7.52	—	—	—	—	—	—	SU
1:8	0.36	0.3170	0.384	6.361	7.51	—	—	—	—	—	—	SU
1:8	0.40	0.3006	0.407	5.373	7.39	1.219	0.570	5.68	5.76	5.91	6.01	SU
1:8	0.60	0.2455	0.592	4.689	6.99	1.392	0.791	5.35	5.41	5.48	5.56	PL

Table 1: Numerical results for computations in Figs. 2-12. $t'_a-t'_d$ denote times of curves a-d in figures 2-5 or 8,9, parts (a)-(c), with $t' = 0$ corresponding to the incident wave crest passing the toe of the slope. Note, $h'_b = 1 - x'_b s$.

s	H'_o	S_o	H_b/h_b	h_b/h_o	Type	Source
1:100	0.20	0.0340	1.00	—	—	CS
1:50	0.20	0.0680	1.28	—	—	CS
1:33	0.20	0.1020	1.52	—	—	CS
1:35	0.10	0.1374	1.93	0.100	PL	GR
1:35	0.15	0.1122	1.50	0.177	PL	GR
1:35	0.20	0.0972	1.36	0.252	PL	GR
1:35	0.15	0.0869	1.34	0.300	PL	GR
1:164	0.40	0.0147	0.967	0.617	SP	PR
1:106	0.35	0.0242	1.015	0.544	SP	PR
1:80	0.20	0.0429	1.073	0.368	PL	PR
1:80	0.30	0.0350	1.086	0.467	PL	PR
1:80	0.40	0.0303	1.071	0.532	PL	PR
1:63	0.25	0.0481	1.102	0.395	PL	PR
1:52	0.20	0.0654	1.222	0.312	PL	PR
1:161	0.40	0.0149	0.840	0.630	SP	SK
1:133	0.20	0.0256	0.910	0.420	SP	SK
1:52	0.20	0.0654	1.240	0.300	PL	SK

Table 2: Experimental results for solitary waves of height H'_o shoaling and breaking over a slope s . CS : Camfield and Street (1969); GR : Grilli *et al.* (1994); PR : Papanicolaou and Raichlen (1987); SK : Skjelbreia (1987).

Appendix V—List of figure captions

Figure 1: Definition sketch for the FNPM computations of a solitary wave of height H'_o shoaling and breaking over a slope s . BP : Breaking point for which the wave front face has a vertical tangent.

Figure 2: Computations for the shoaling of solitary waves with, $H'_o =$ (a) 0.20; (b) 0.40; (c) 0.60, on a slope $s = 1:100$. Times of curves a-d are given in Table 1. Curves a in parts (a)-(c) correspond to the BP. Part (d) shows a superposition of curves d from parts (a)-(c), scaled by H'_o and translated to the crest location x_c .

Figure 3: Same as Fig. 2 for $s = 1:35$.

Figure 4: Same as Fig. 2 for $s = 1:15$ and $H'_o =$ (a) and a' : 0.30; (b) and b' : 0.45; (c) and c : 0.60.

Figure 5: Same as Fig. 2 for $s = 1:8$, except that breaking does not occur in part (a) and that curve a in part (a) is used as curve a in part (d).

Figure 6: Shoaling of solitary waves of initial wave heights $H'_o =$ (a) 0.20; and (b) 0.60, on slopes of $s =$ a: 1:100; b: 1:35; c: 1:15; and d: 1:8. Scaled curves are directly imported from Figs. 2d-5d, except for curve c in part (a) which has been recalculated.

Figure 7: Shoaling curves for computations in Figs. 2-5 : $s =$ (- - - -) 1:100; (—) 1:35; (— - —) 1:15; (— —) 1:8. Symbols (o) denote the BP. G : Green's law; B : Boussinesq's law.

Figure 8: Computations of the transition to breaking, with $H'_o =$ (a) 0.06; (b) 0.08; (c) 0.10, on a slope $s = 1:15$. Times of curves a-d are given in Table 1. Part (d) shows a superposition of curves a from part (a) and curves d from parts (b) and(c), scaled by H'_o .

Figure 9: Same as Fig. 7, with $H'_o =$ (a) 0.22; (b) 0.26; (c) 0.30, on a slope $s = 1:8$.

Figure 10: Computational results from Table 1 as a function of wave height H'_o and slope s : (◇) SU; (o) PL; (●) SP; (—) breaking criterion (1); (- - - -) NSW breaking criterion; (- - - - -) parameter S_o from equation (3).

Figure 11: Combination of breaking criterion, breaking depth and indices, for incident waves H'_o on a slope s , with : (—) curve fits to computations : (a) (5) and (b) (6),(7); (- - - -) curve fits to experiments. Numerical data in Table 1 are represented by : (o) SP-PL and (◇) SU. Experimental data in Table 2 are represented by : (a) (●) PL and (△) SP; (b) (●) SP-PL.

Figure 12: The empirical values of the breaker index determined from : (a) (- - - -) CS index (4)

and (—) (5) for $H'_o =$ a: 0.05, b: 0.10, c: 0.20, d: 0.30, e: 0.40, f: 0.50, g: 0.60, h: 0.78; (b) (—) (5) where upper numbers on curves denote constant values of H_b/h_b and lower numbers constant values of \mathcal{S}_o .

Appendix VI—Figures

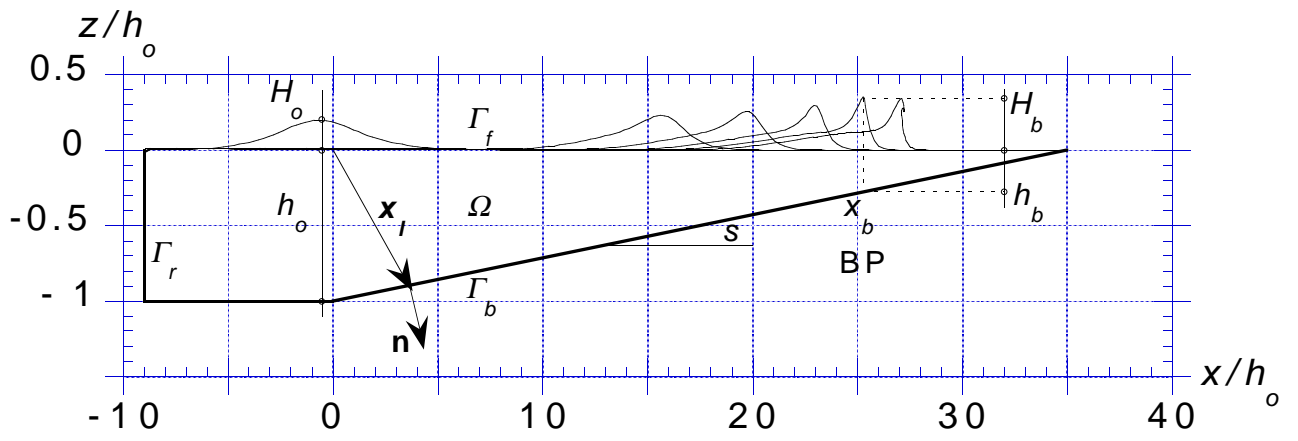


Figure 1:

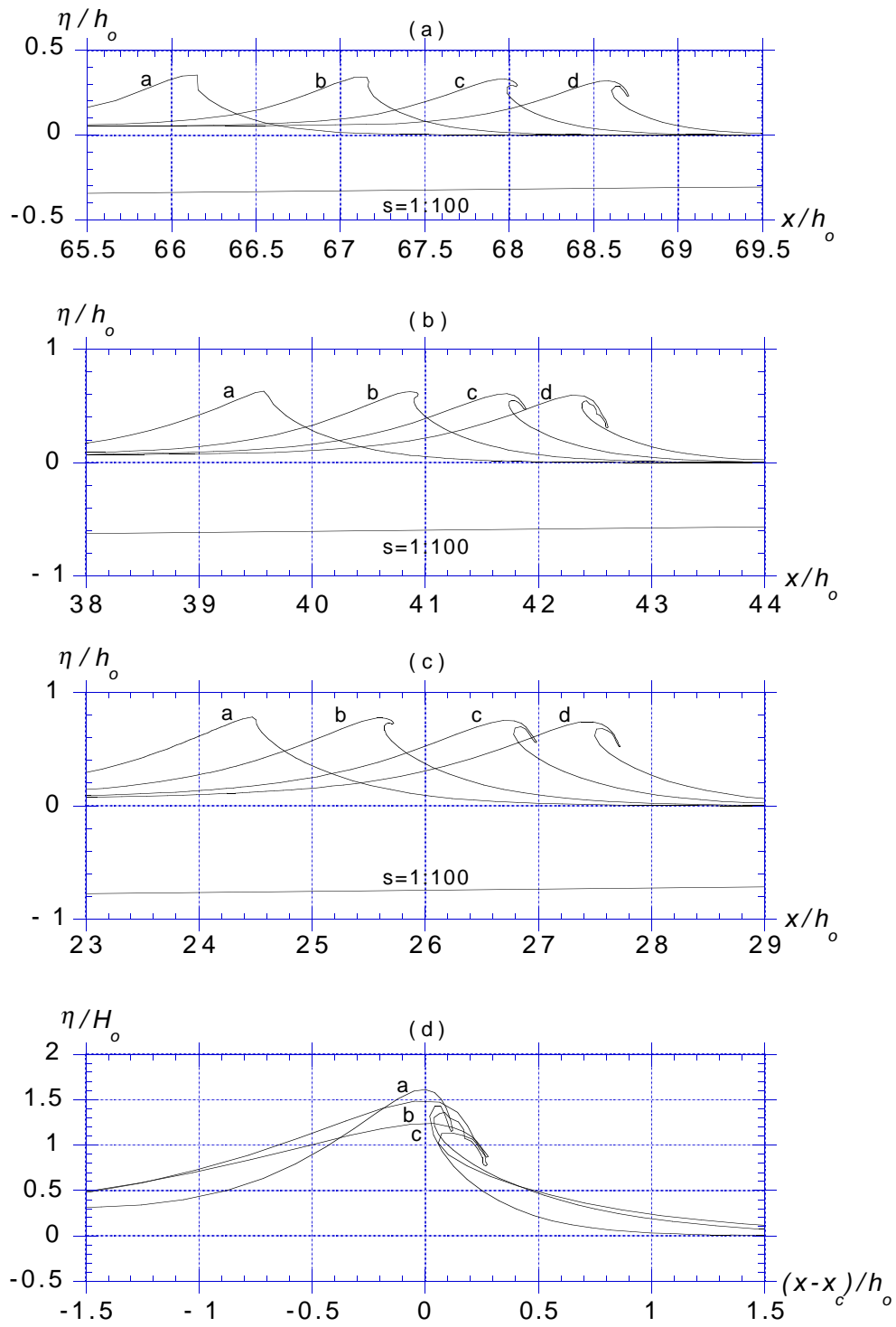


Figure 2:

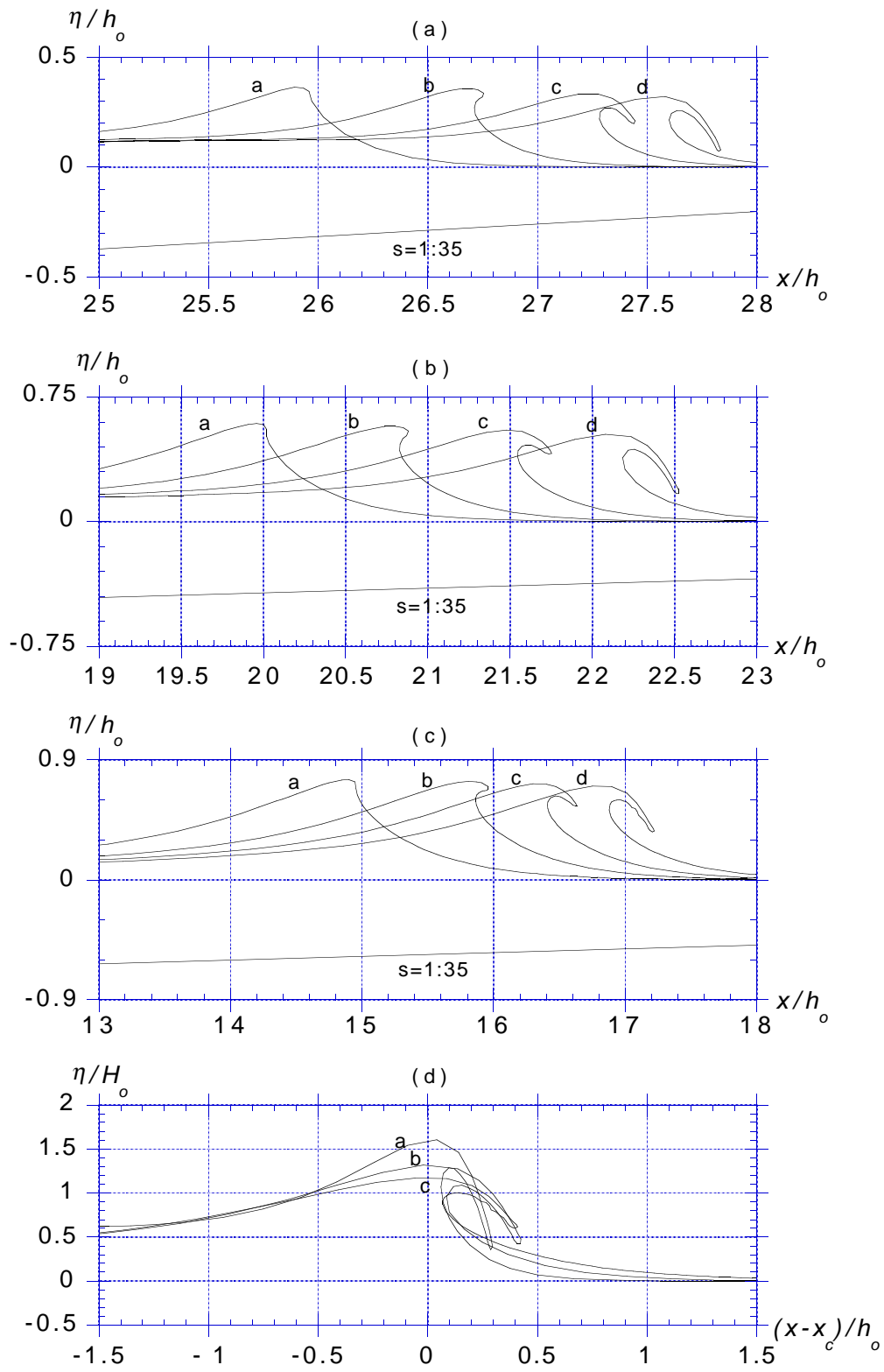


Figure 3:

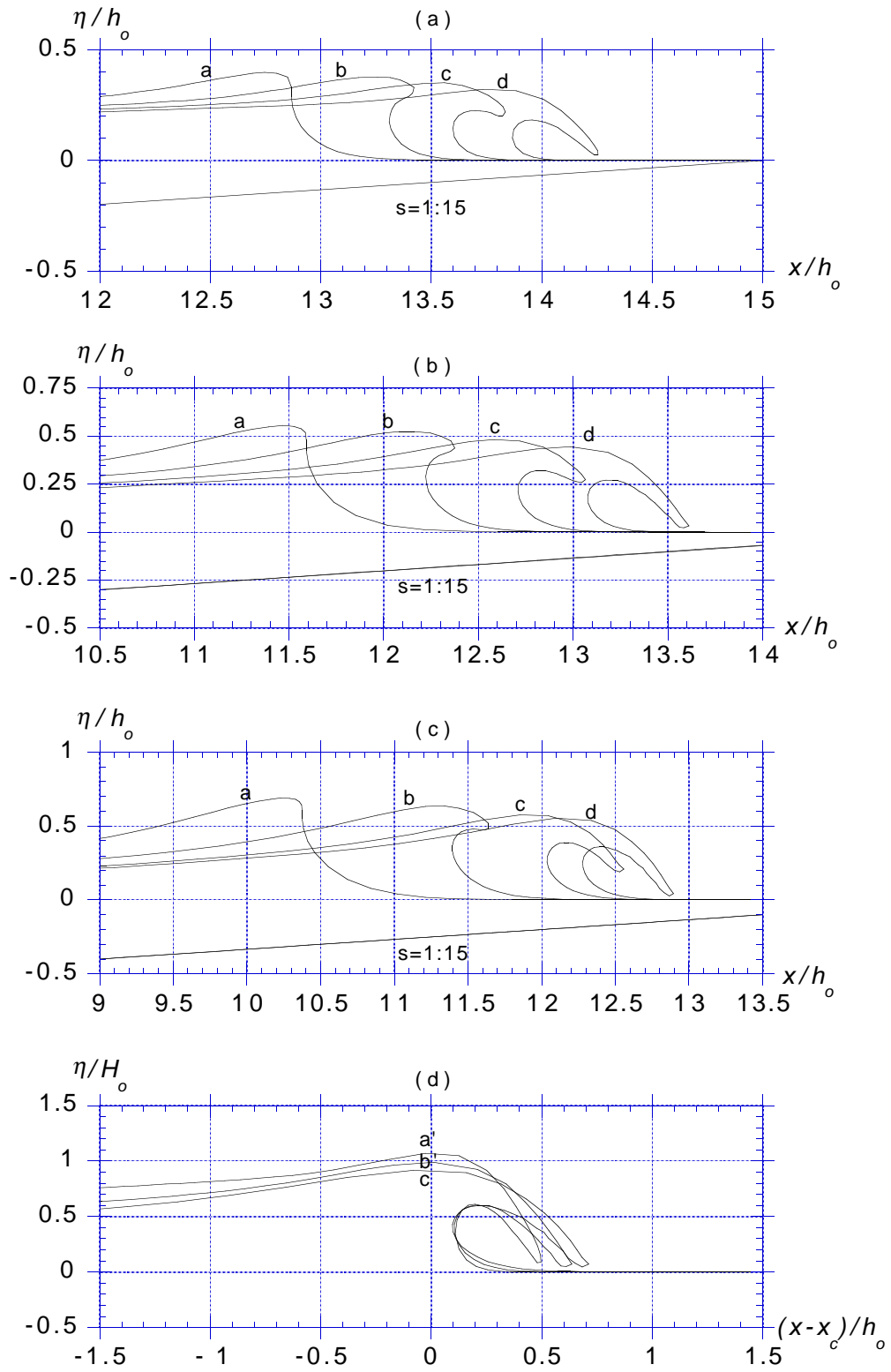


Figure 4:

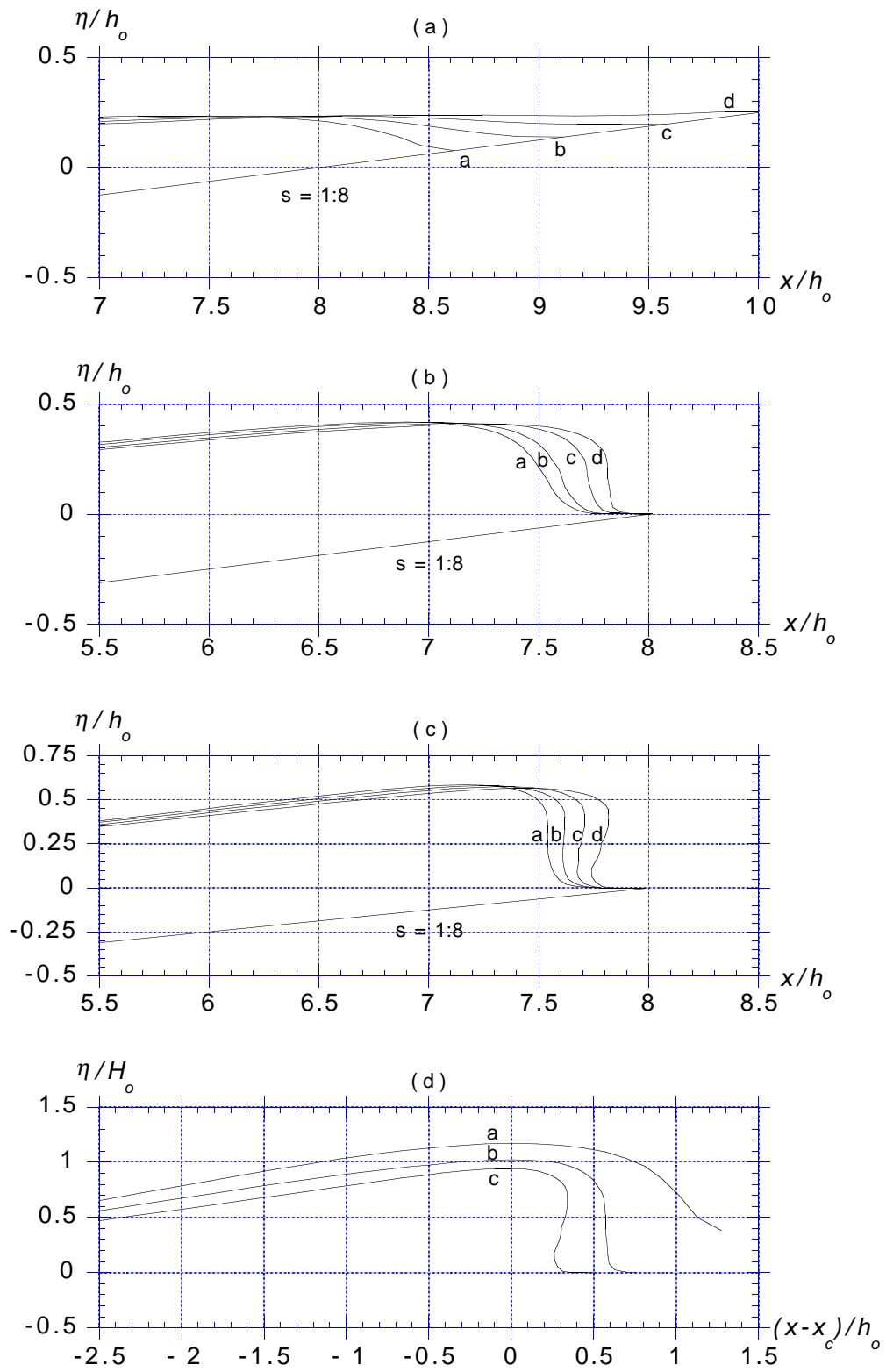


Figure 5:

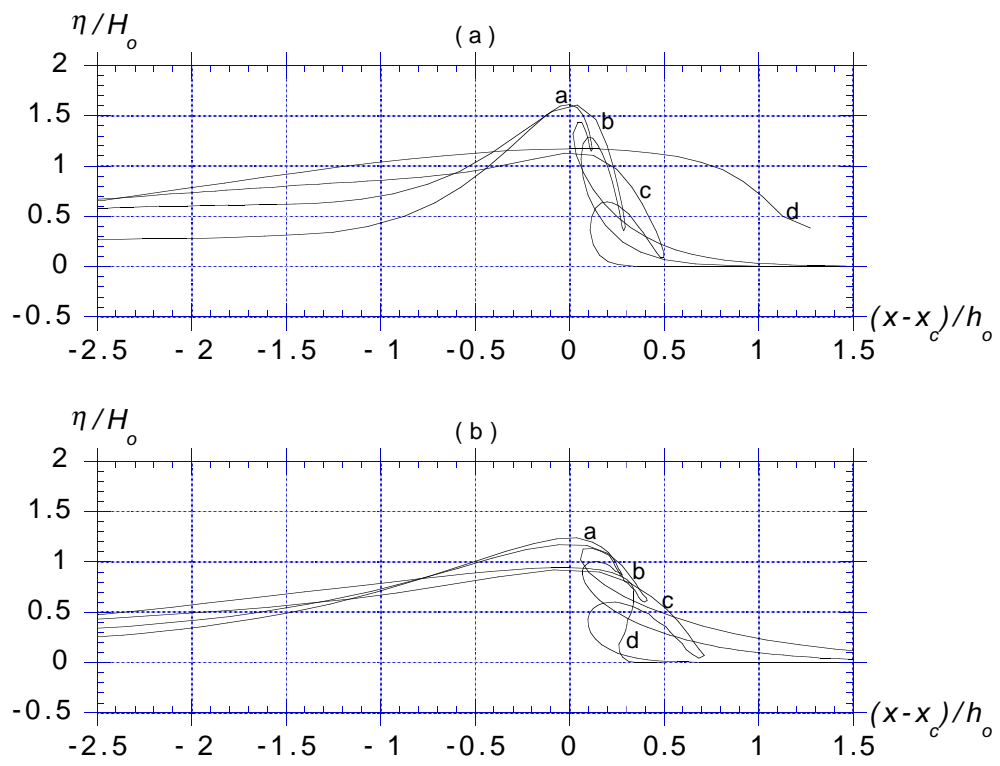


Figure 6:

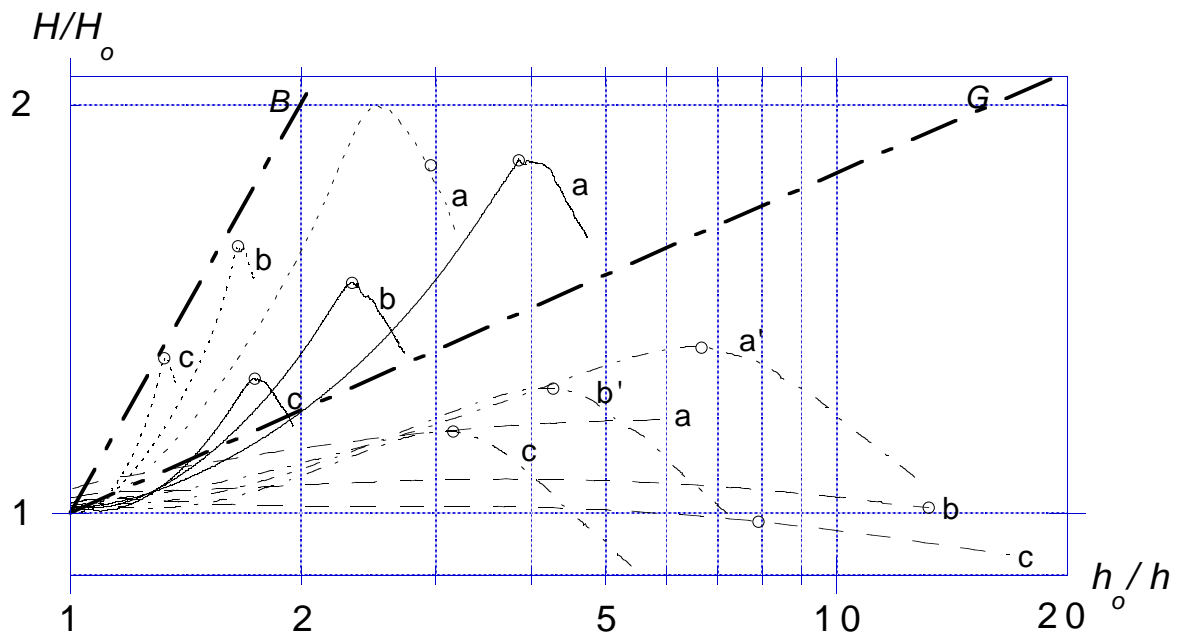


Figure 7:

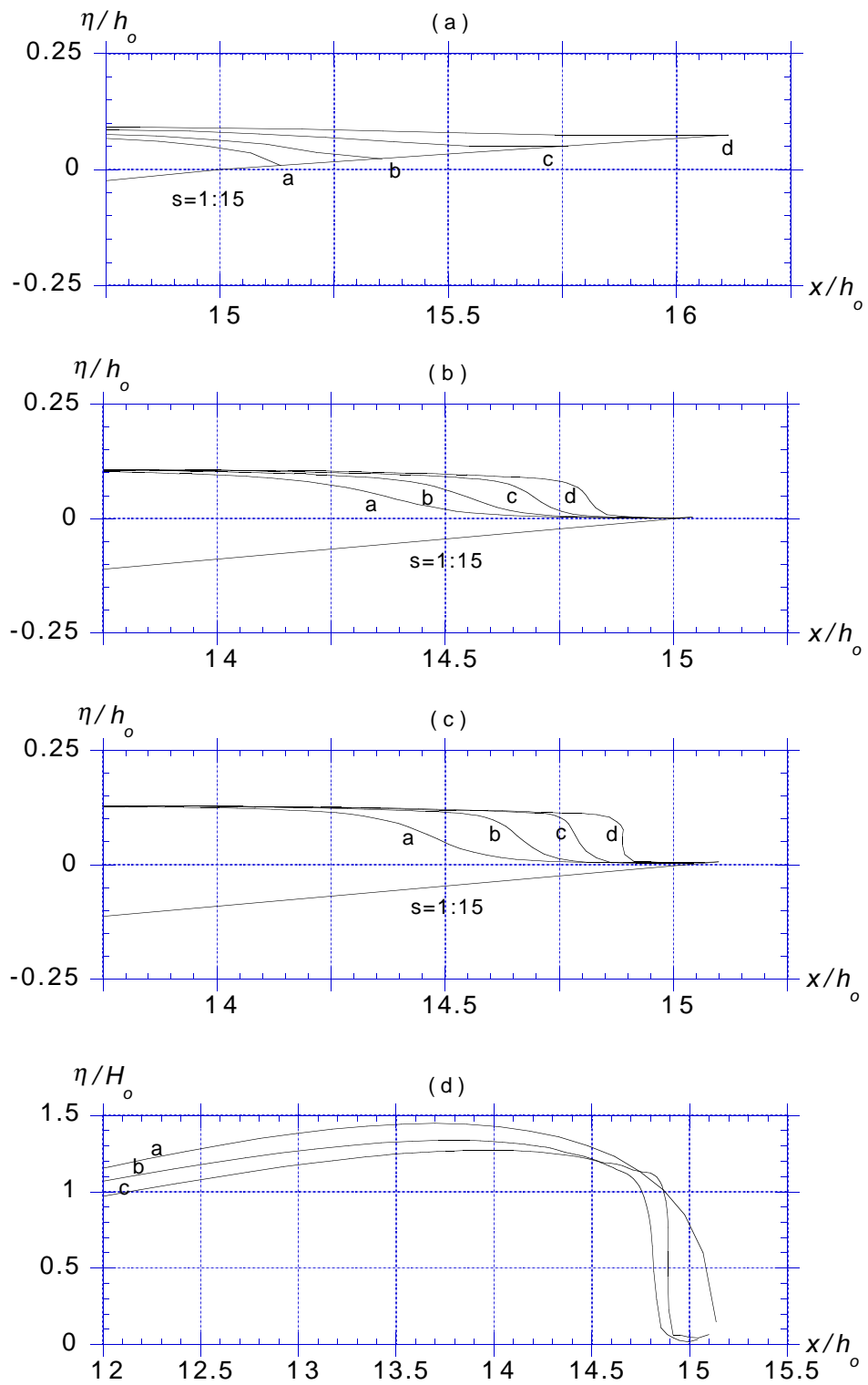


Figure 8:

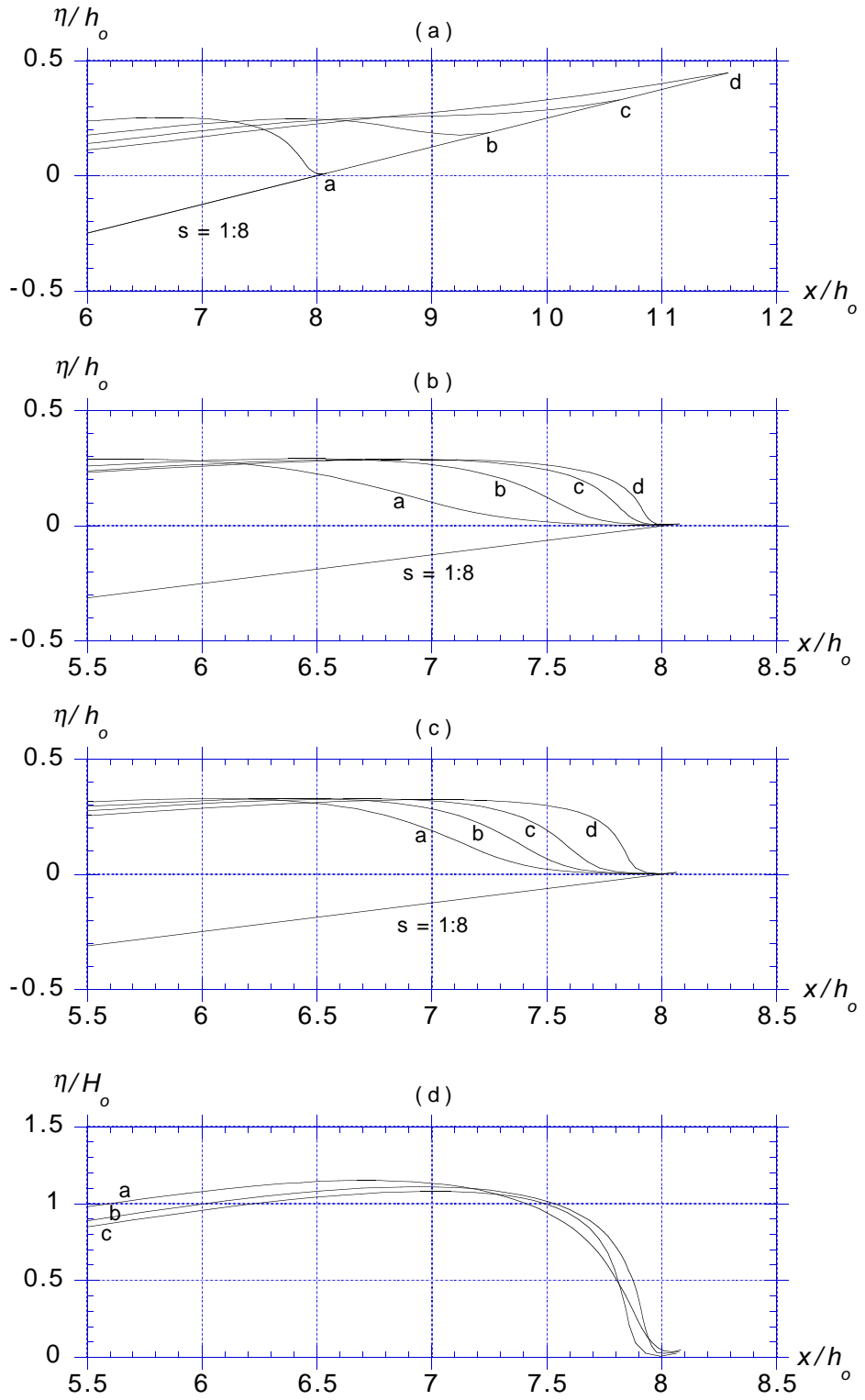


Figure 9:

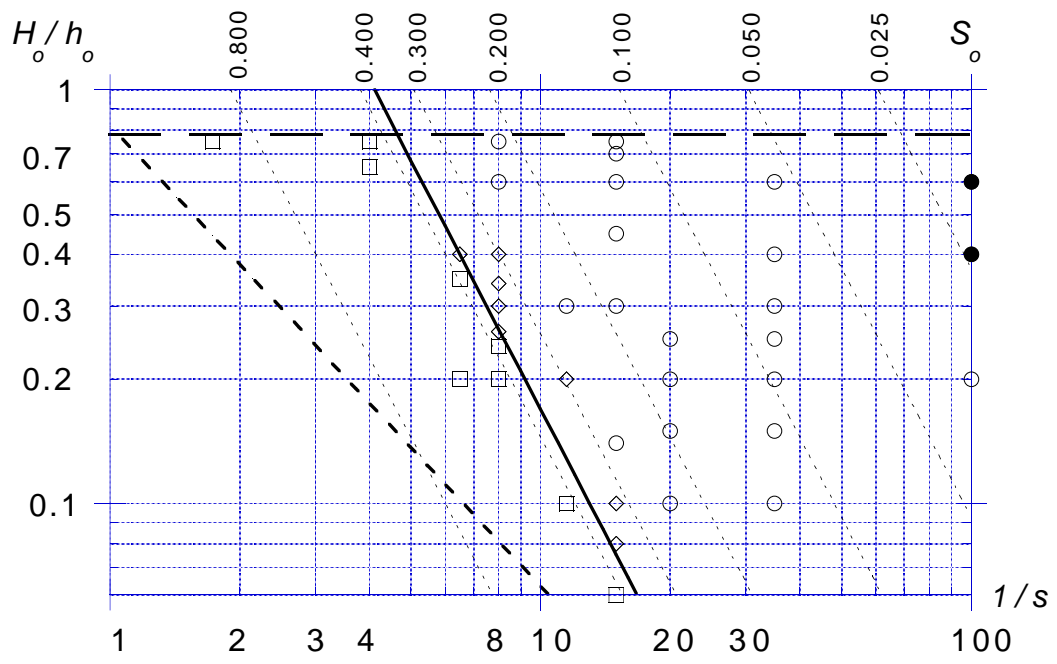


Figure 10:

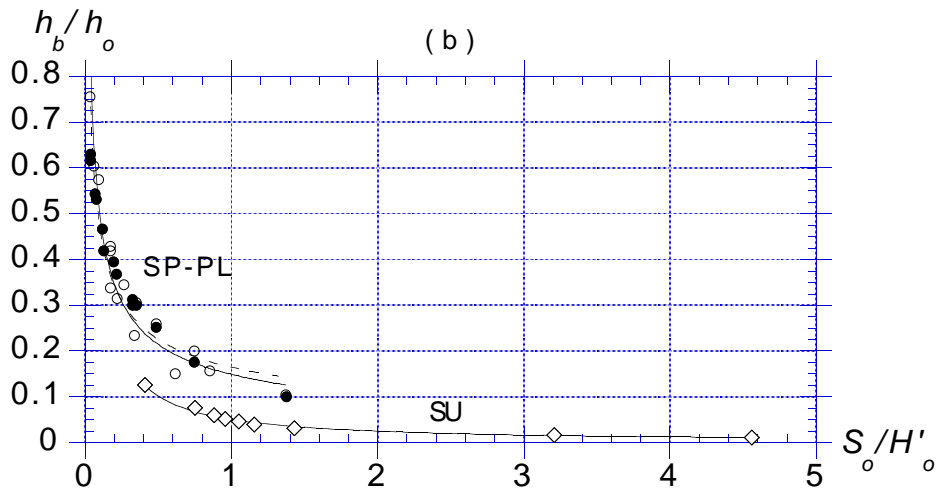
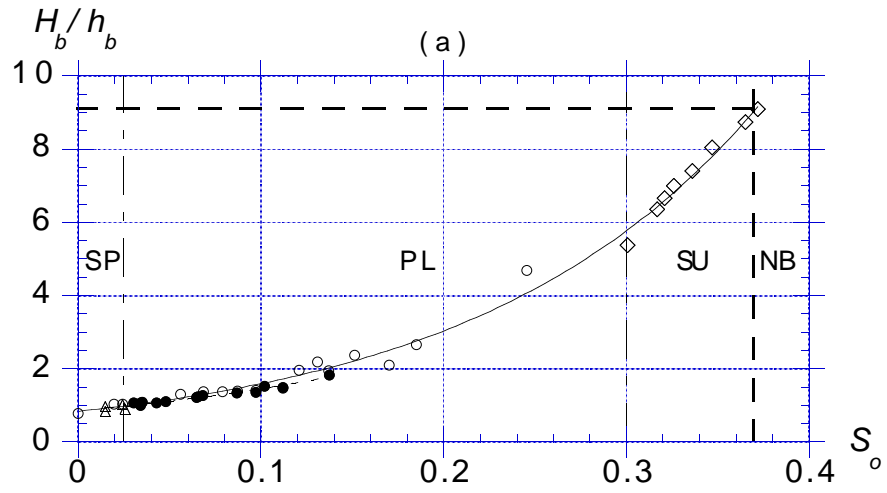


Figure 11:

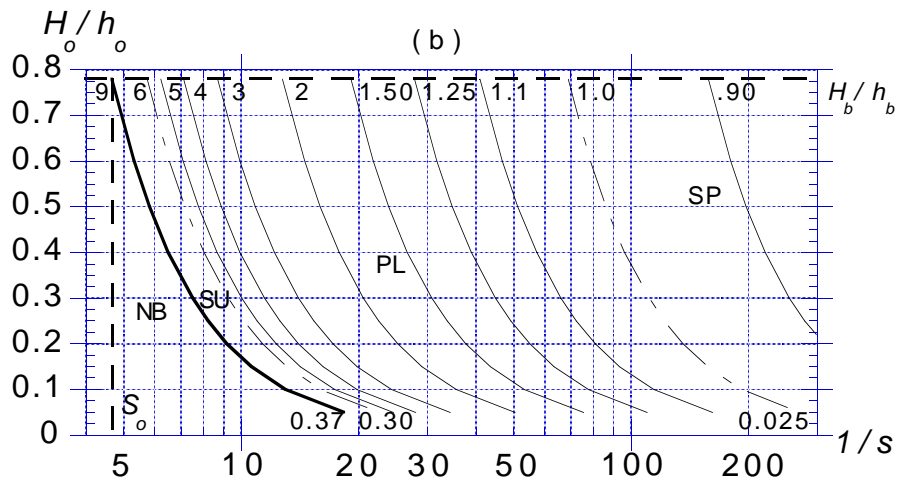
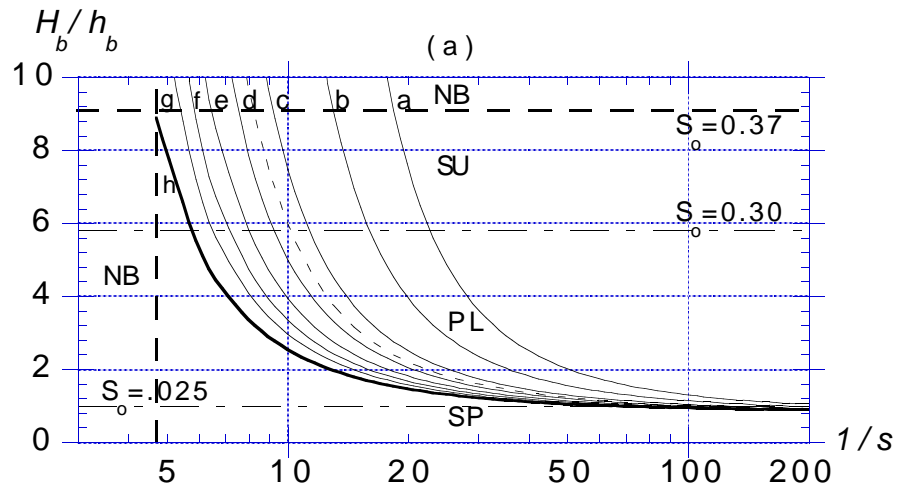


Figure 12: